CO oxidation at low temperature on Au/CePO4: Mechanistic aspects

F. Romero-Sarria, M.I. Domínguez, M.A. Centeno, J.A. Odriozola

Departamento de Química Inorgánica e Instituto de Ciencia de Materiales de Sevilla, Centro Mixto Universidad de Sevilla-CSIC, Avda. Américo Vespucio 49, 41092 Sevilla, Spain

Abstract

This work reports the synthesis and characterization of a cerium phosphate supported gold catalyst as well as its catalytic activity for the oxidation of CO. A precipitation method in the presence of an organic modifier followed by a hydrothermal treatment was used for the support synthesis, resulting in high surface area nanometric particles. Gold/cerium phosphate catalyst with a 1% (w/w) nominal gold content was characterized using XRF, XRD, N2 adsorption–desorption measurements, TEM and DRIFTS-MS. The catalyst shows good catalytic activity at low temperature. The activity is related to the generation of oxygen vacancies in the support caused by the elimination of structural oxygen. In situ studies revealed that the reaction of the oxygen vacancies with gaseous oxygen resulted in the formation of peroxo species. These species are responsible for the activity detected at room temperature in both the catalyst and the support. Moreover, the presence of carbonate and hydrogen carbonate acting as reaction intermediates have been observed

Graphical abstract

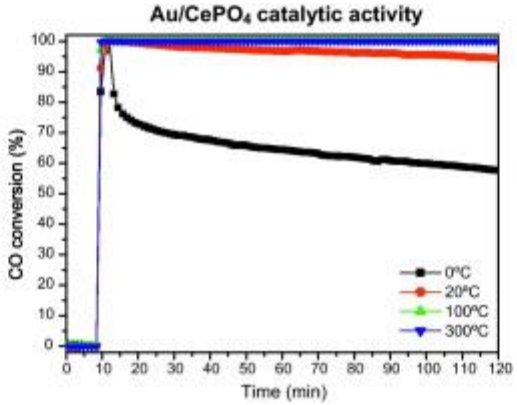

Highlights

CePO4 (rhabdophane structure) is used as support of gold catalysts for CO oxidation. Dehydration of the support during activation induces oxygen vacancies generation. Oxygen vacancies are able to react with gaseous oxygen to give peroxide species. Peroxides oxidize CO at low temperature giving carbonates that poison surface sites. By rising temperature, when gold is present, carbonates decompose and activity rises.

Keywords

Gold; Cerium phosphate; CO oxidation; DRIFTS; Peroxides

1. Introduction

Carbon monoxide is a hazardous gas mainly generated in incomplete combustion processes [1]. Therefore, its catalytic abatement results highly attractive and has been the object of a great number of works in the last years [2], [3], [4], [5], [6], [7], [8], [9] and [10]. The role of reaction conditions in the CO oxidation reaction over gold catalysts [5], the nature of the active species [6] and [7], the reaction mechanism and the role of the support [8], [9] and [10], among others factors, are found in the literature.

As a result of these and other works some statements are well established in the scientific literature. Among them, the support classification proposed by Schubert et al. [8] as "active" or "inert" supports, as a function of their reducibility is particularly important. According to these authors, gold particle size is the main factor determining the catalytic activity gold particles supported on inert supports, since in these catalysts, gaseous O2 is dissociated on the metallic particle. On the contrary, oxygen activation proceeds on the support for gold catalysts supported on active materials and, therefore, the gold particle size is not the main factor determining the catalytic activity. Liu et al. [11] proposed that the adsorption of molecular oxygen in active support results in superoxide species nucleated at the support oxygen vacancies. This explains the high mobility of active oxygen at the surface, thus favoring the rate-determining step of this reaction.

In previous works we have observed the formation of peroxide species during the CO oxidation reaction on a gold catalyst deposited on an inert support. Anionic vacancies, having high electronic density, transfer the excess charge to molecular oxygen adsorbed on them resulting on the formation of peroxide species [12]. A stoichiometric CO oxidation process occurs at room temperature (CO conversion close to 100%) between adsorbed peroxide species, formed by adsorption of molecular oxygen on oxygen vacancies of the support, and carbon monoxide.

In this work, a gold catalyst deposited on cerium (III) phosphate, an inactive support, was synthesized and characterized. Light-off curves for the oxidation of CO were obtained for both the catalyst and the support. A complementary set of experiments in isothermal conditions (0, 20, 100 and 300 °C), as well as DRIFTS-MS in situ experiments were designed to highlighten aspects of the reaction mechanism.

2. Experimental

Phosphoric acid 85% (Panreac), cerium (III) nitrate hexahidrate (Alfa), ammonia 30% (Panreac), sodium citrate dihydrate (Panreac) and hydrogen tetrachloroaurate (Alfa) were used for synthesizing the studied solids.

Solutions of phosphoric acid and cerium (III) nitrate of similar concentrations were mixed and maintained at 40 °C in a thermostatic bath while stirring. To this solution an aqueous solution of sodium citrate (5.68 g L−1) was added and the pH of the obtained solution adjusted to 10 by adding adequate amounts of ammonia, during all these

processes the mixture was thoroughly stirred. The solution was kept at 40 °C for 8 h up to reaction completion. The resulting mixture was hydrothermally aged at 100 °C for 8 h. The solid fraction resulting in this process was filtered off, thoroughly washed with distilled water until reaching pH 7 and finally dried overnight at 100 °C. The catalytic support obtained by this procedure will be referred as CeP.

A deposition–precipitation process was used to prepare the gold-cerium phosphate catalyst, denoted as AuCeP. The required amount of HAuCl4·3H2O for synthesizing 1% by weight gold catalyst was dissolved in distilled water and the pH adjusted to 9 with NaOH 0.1 M. The solution was heated at 65 °C and then the support was added, keeping the mixture under vigorous stirring at 65 °C for 1 h [13]. After this, the catalyst was separated by filtration, washed with deionised water to remove chloride and Na+, and dried overnight at 100 °C.

The CO oxidation reaction was carried out in a conventional U-shaped reactor working at atmospheric pressure. In a typical run, 80 mg of sample (particle size 100–200 μm) were placed into the reactor between two plugs of glass wool. The catalyst was activated under a total flow of 30 mL min−1 (21% O2 in He), the temperature increased at 300 °C (10 °C min−1) and maintained at this temperature for 1 h. The reactor was surrounded by an electrical furnace equipped with a temperature programmer. A thermocouple in contact with the sample assures the right measure of the temperature. Then, the reactor was cooled down to room temperature in the oxidative flow. Light-off curves for CO oxidation were obtained from RT to 300 °C at a heating rate of 5 °C min−1. A mixture containing 3.4% CO (Air Liquide, 99.997% pure, <3 ppm H2O) and 21% O2 (Air Liquide, 99.999% pure, <3 ppm H2O) in He (Air Liquide, 99.999% pure, <3 ppm H2O) at a total flow rate of 42 mL min−1was used for all the catalytic tests. Empty reactor (without catalyst) shows no activity under such conditions. Catalytic activities as a function of time on were also measured in isothermal conditions at 0, 20, 100 and 300 °C using the same reaction mixture and total flows. The reaction products were analyzed by mass spectrometry, using a Balzers Thermostar benchtop mass spectrometer controlled by the software Balzers Quadstar 422 with capabilities for quantitative analysis.

Chemical compositions of the obtained materials were measured by X-ray fluorescence (XRF), employing a PANalytical AXIOS sequential spectrophotometer with a rhodium tube as source of radiation. XRF measurements were performed onto pressed pellets (sample including 6 wt.% of wax).

X-ray diffraction (XRD) analysis was carried out on a Siemens diffractometer D500. Diffraction patterns were recorded with Cu Kα radiation (40 mA, 40 kV) over a 2θ range of 10–70°and a position-sensitive detector using a step size of 0.05° and a step time of 1 s.

The textural properties were studied by N2 adsorption–desorption measurements at liquid nitrogen temperature. The experiences were performed in a Micromerits ASAP

2010 equipment. Before analysis, the samples were degassed for 2 h at 150 °C in vacuum.

Transmission electron microscopy (TEM) observations were carried out in a Philips CM200 microscope operating at 200 kV. The samples were dispersed in ethanol by sonication and dropped on a copper grid coated with a carbon film.

In situ DRIFTS-MS studies were carried out during the activation and reaction steps of the catalyst. DRIFT spectra were obtained in a Thermo Nicolet Nexus infrared spectrometer with a KBr optic and a MCT/B detector working at liquid nitrogen temperature. An environmental DRIFTS chamber (Spectra-Tech 0030-101) is equipped with ZnSe windows, allowing in situ treatments up to 500 °C and 1 atm. The gaseous flow coming from the cell was analyzed by the mass spectrometer previously described. The sample was placed inside the chamber without packing or dilution. The spectra of the samples during the activation and the reaction processes (different atmospheres and temperatures), were obtained by co-adding 64 scans at 4 cm−1 resolution. The spectrum obtained for an aluminum mirror was used as background.

3. Results and discussion

By adding organic chelating agents to the solutions containing phosphate anions and metallic cations Wang et al. [14] have reported the preparation of nanometric hydroxyapatites crystals. In this paper we have adapted their method to produce high surface area nanometric crystals of cerium phosphate.

The chemical composition (wt. %) of both the cerium phosphate support and the gold catalyst are given in Table 1. The gold content measured by XRF, is very close to the target one.

The synthesized support presents, after drying at 100 °C, a diffraction pattern matching the one corresponding to the rhabdophane phase (JCPDS-ICDD 75-1880), a hexagonal structure of cerium (III) phosphate, Fig. 1. In order to determine the presence of amorphous phases undetected by XRD, the support was calcined at 950 °C for inducing crystallization of amorphous oxides if present [15] and their crystalline structure was further determined. The XRD pattern of the calcined support, Fig. 1, shows the presence of diffraction lines corresponding to monazite, monoclinic structure of the cerium (III) phosphate, (JCPDS-ICDD 32-0199) and diffraction lines of very low intensity associated to cerianite (CeO2) phases (JCPDS-ICDD 43-1002), although this later phase just account for as much as 2% of the final solid as estimated by the intensity of the diffraction lines, which roughly accounts for the chemical composition deduced by FRX, Table 1. Therefore, the effect of the cerianite phase in the overall catalytic activity of the solid may not be taken into consideration. The transformation of the rhabdophane structure into monazite upon calcining at moderate temperatures has been previously reported [16].

Structural modifications of the support (CeP) are not observed after gold deposition, since the diffraction lines corresponding to the support remain unaltered. The diffraction lines corresponding to metallic gold overlap those corresponding to the CePO4 phase, preventing the estimation of gold particle size based on diffraction line broadening. However, an estimate of the particle size of both the support and the active phase may be obtained from TEM data. Acicular nanometric crystals of cerium phosphate reaching roughly 100 nm in length form the support, Fig. 2A. The gold-supported catalyst shows the same morphology for the phosphate phase but the presence of few gold spherical particles with diameters below 5 nm, Fig. 2B. As gold particles resulted undetectable by SEM, gold agglomeration in big particles must be ruled out. Therefore, as the amount of gold particles detected by TEM is fairly low for a 1% by weight gold loading, particle sizes for gold well below 5 nm in diameter must be assumed.

The textural properties of both the support and the catalyst are summarized in Table 1. Both solids present N2 adsorption–desorption isotherms corresponding to type IV with H2-type hysteresis loop according to the IUPAC classification. This pointing to a pore system formed by a complex structure of interconnected pores with different shapes and sizes. Gold deposition results in a small decrease of surface area while slightly increasing pore diameter. Somorjai and co-workers obtained similar results for gold nanoparticles modified mesostructured silica materials MCM-41 and MCM-48 [17], explaining their results by the introduction of gold nanoparticles in the pores resulting in turn in the expansion of the mesoporous structure.

Fig. 3 shows the light-off curves for CO oxidation over both the support and the gold catalyst. A high CO conversion peak, ca. 70% CO conversion, that suddenly falls to zero conversion is observed for the support at room temperature, the support become again active for temperatures above 175 °C reaching 10% CO conversion at the highest temperature tested in this study, 300 °C. The gold catalyst, however, shows 100% CO conversion in the whole range of temperatures from RT to 300 °C.

The catalytic activity of the gold catalyst was studied in isothermal conditions at 0, 20, 100 and 300 °C keeping the catalyst in the reaction stream for 2 h (≈100 cycles), Fig. 4. Whatever the temperature, 100% initial CO conversion is observed, the catalyst remains active without loosing activity at the highest temperatures studied, however an activity decrease is observed after 2 h under reactive flow when the temperature is set at 0 °C or 20 °C, being this decrease bigger in the former case.

Since initial total conversion of CO is observed at RT for both the catalyst and the cerium phosphate support, one can think this behavior is due to phenomena produced on the support, which are enhanced by the presence of gold. In order to shine light on the species responsible of this activity, the catalysts behavior was analyzed during the activation and the reaction by in situ DRIFTS-MS studies. The main objective of this study is to determine some aspects such as: the species responsible for the high activity observed at room temperature; the effect that provokes a deactivation of the catalyst

with time, if the temperature is lower than 100 °C, and the role of the gold in this catalytic system.

3.1. Catalyst activation

Catalyst activation results in the evolution of water as observed by mass spectrometry, Fig. 5. Three main water desorption processes are observed at RT, 150 °C and 230 °C. These desorption peaks are correlated with the structural modifications undergone by the solid during the activation process. Difference IR spectra, the spectrum corresponding to the fresh solid is taken as reference, are obtained for the whole activation protocol. Fig. 6 presents the spectra corresponding to the solid after finishing each of the observed water desorption processes. For the sake of comparison, the spectrum corresponding to the final stage of the activation is included in order to detect possible modifications occurring in isothermal condition at the activation temperature.

Water elimination at room temperature induces surface modifications, which are enhanced as temperature increases. Negative bands at 1630 and 3700 cm−1 due to water and H-bonded surface hydroxyl groups loss respectively [18], appear upon dehydration. Special attention has to be paid to the band at 750 cm−1. According to Assaaoudi et al. [19] this band is due to the librational mode of water molecules in rare earth orthophosphates. This mode of vibration has also been observed in zeolites, crytomelanes and hydroxyapatite [12], [20] and [21], materials with structural channels containing water molecules. Therefore, the negative band at ca. 750 cm−1 clearly indicates the elimination of water molecules from structural interstices.

A band at 1154 cm−1 also disappears while two new features at 1217 and 1094 cm−1 attributed to ν3(PO4) modes [22] appear. According to Mooney [16], Ce3+ cations are bonded to eight oxygen atoms and each phosphate group is linked to six Ce3+ ions in the hexagonal structure of the cerium phosphate (rhabdophane). This structural arrangement results in open channels along the c axis. The water molecules placed in the interstices stabilize the structure. Therefore, a modification of the structure is expected if the solid is treated thermally (dehydration) at moderate temperatures. Since the modification of the symmetry entails a change in number and position of the IR active modes [23], it is clear that dehydration of the solids is associated with the modification of the phosphate groups, in good agreement with the reported data.

A band at 3668 cm−1 is observed whatever the temperature, which, according to previous data, may be due to P–OH groups [24] or to hydroxyls groups associated to Ce3+ sites [25]. The IR spectra suggest that water molecules elimination from the interstices results in changes in phosphate group symmetry together with the generation of OH groups. Upon dehydration under vacuum at room temperature it has been described that the CePO4 structure does not change although their stability decreases [16]. In this structure, the available spaces for water may be described as cylindrical, oxygen-lined tunnels of diameter 5.3 Å. The oxygens are distributed roughly in rings at intervals of one-third of the c axis. The points (0, 0, 1/2), (0, 0, 5/6), and (0, 0, 1/6) lie half-way between these rings and are at distances of 2.85 Å from the eight nearest

oxygen atoms. These crystallographic sites may accommodate ions of moderate size, upon dehydration, if the charges were compensated in some way. Therefore, a breakdown of Ce–O–P bridges with formation of a vacancy and CeIII–OH bonds, as suggested by our IR data, is compatible with the crystallographic description of the CePO4 structure and its modification upon dehydration. Considering that these ions are initially interacting with the "O" sites of the phosphate groups, it must be considered that oxygen vacancies generation is strongly possible in the studied conditions, probably associated to the P atoms, being the OH associated to the Ce3+.

3.2. Reaction

On submitting the activated catalyst to the CO + O2 stream at room temperature CO2 evolution is immediately observed (Fig. 7). A band at 2350 cm−1 corresponding to CO2 adsorbed on the surface [26] confirms this fact. IR spectra were taken under reaction conditions at different temperatures and adsorbed species under actual reaction conditions determined by analyzing difference spectra, taking the spectrum of the activated solid as reference. Positive bands, indicating appearing species at 1679, 1617, 1405, 1218 and 1154 cm−1 evolve at RT. Moreover, two new positive features at 3610 and 3713 cm−1 and a negative band at ca. 3670 cm−1 are observed in the O–H stretching region.

The set of bands observed in the 1700–1200 cm−1 region correspond to carbonate and hydrogen carbonate species [27]. Specifically, bands at 1599 and 1413 cm−1 have been assigned to ν(C–O) mode of hydrogen carbonate species on ceria. According to the same authors, bands at 1567 and 1289 cm−1 are detected when bidentade carbonates are formed on the ceria surface, while the monodentade carbonate shows bands at 1504 and 1351 cm−1. The bands at 3610 and 1218 cm−1 accounts for the ν(OH) and δ(OH) modes of hydrogen carbonate, respectively, while the band at 3713 cm−1 is assigned to the O–H stretching mode of P–OH species [12]. These bands confirm the formation of these species through the interaction of CO2 with surface O2− and OH sites [28]. Hydrogen carbonates are formed at the expenses of the hydroxyl species responsible for the band at ca. 3670 cm−1. This band is assigned to hydroxyls groups bonded to Ce3+ sites formed during the activation step. Therefore, CO oxidation to CO2 occurs at room temperature with the formation of carbonate species.

Li et al. [26] study the catalytic oxidation of CO on FePO4. These authors used isotopically labeled oxygen for establishing the reaction mechanism. According to these authors, CO oxidation takes place either by active bulk oxygen that reacts with CO adsorbed on gold sites, or by gas phase oxygen activated on reduced gold sites. Whatever the mechanism, they found that a reduction pretreatment enhances the catalytic activity in the CO oxidation reaction. It must be considered that molecular oxygen activation requires surface sites having negative density of charge to be transferred to gaseous oxygen molecules. O2 molecules accept electrons in antibonding orbitals (π*); this reduces O–O bond order, weakens the O–O bond and favors the formation of active oxygen species [8].

Prior to reaction, the CePO4 catalyst was activated at 300 °C for 1 h in an O2-rich helium flow reducing the probability of finding Auδ− sites. Moreover, the CO conversion peak appearing at room temperature when the reaction is carried out in the support suggests active species other than gold as the active ones at room temperature. The formation of oxygen vacancies during the activation step generates surface sites with high electron density (formally one electron trapped in a vacancy) that react with gas phase molecular oxygen resulting in adsorbed suboxide species (peroxide or superoxide) species, which are strongly oxidizing agents. These species have been previously observed in hydroxyapatite structures [12]. Therefore, oxygen vacancies, formed in the catalyst activation process, may play a key role in the reaction mechanism; negatively charged molecular oxygen adsorbed in a surface vacancy reacts with adsorbed CO giving rise to the adsorbed carbonate species observed at room temperature.

On increasing the reaction temperature, the intensity of the bands corresponding to carbonates and hydrogen carbonates species decrease and these later bands finally disappears at the highest temperature tried while CO conversion increases, Fig. 7. Bicarbonate species are the first ones in decomposing, which is in accordance with the thermal stability of these species and the observed evolution of the bands. Carbonate species remains adsorbed at 300 °C; these species are characterized by a set of bands in the 1350 cm−1 region and a broad band at ca. 1510 cm−1; considering the frequencies of the bands and the treatment temperature, these bands may be attributed to polydentate carbonate species [27] that is in agreement with the highest stability of polydentate carbonate species with respect to bidentate and bridged ones. The band at 1154 cm−1 observed in Fig. 7 upon heating at 300 °C must be associated with phosphate species. The recovery of this band (disappeared during the activation and attributed to P–O vibrations) indicates that the initial symmetry of the phosphate groups is restored as the reaction proceeds. Therefore, the oxygen vacancies generated upon activation, which results in the symmetry modification causing the disappearance of the 1154 cm−1 band are eliminated at 300 °C. Oxygen activation in gold catalysts supported in active supports occurs at the support surface. This fact is used to explain the high mobility of the active oxygen in the surface, so favoring the rate-determining step of this reaction. Liu et al. [11] postulated the formation of superoxide species at oxygen vacancies, Bond and Thomas proposed as the essential feature of the mechanism for the CO oxidation reaction over gold on TiO2or other reducible oxides the adsorption of O2 on an oxygen vacancy, resulting in the formation of a superoxide species and the reoxidation of the undercoordinated metal cation [29] and [30] and, more recently, Laguna et al. [31] showed the activation of oxygen species at high electronic density surface sites. Besides this, active species formed by transferring electrons from the catalyst to molecular oxygen resulting in peroxide species have been observed during the reaction of CO in a catalyst with an “inactive” support [12].

The occupation of oxygen vacancy sites by molecular oxygen adsorption may result in restoring the symmetry of phosphate groups allowing the recovery of the 1154 cm−1

band while activating the absorbed oxygen through the formation of adsorbed suboxide species. In order to verify this idea, a detailed analysis of the low wavenumber region is performed, Fig. 8.

The π(CO3) modes of carbonate and hydrogen carbonate species appear in the 850–820 cm−1 region, as well as the vibrational modes of peroxide species that show a characteristic band between 800 and 900 cm−1[32]. As observed in Fig. 8, upon heating, bands at 1679, 1617, 1405 cm−1 corresponding to carbonate/hydrogen carbonate species vanish; however, the intensity of the band at 830 cm−1 increases with temperature, pointing to a species responsible for this band different from CO3/HCO3− and, therefore, ascribed to peroxide species [12] and [33]. The intensity of the bands at 830 and 1154 cm−1 follows parallel trends, which indicates that the appearance of peroxide species and the recovery of the symmetry of phosphate groups are simultaneous processes. Therefore, the presence of these species (O22−) explains the high activity observed at room temperature (activation of the gaseous oxygen), and the recovering of the symmetry of the phosphate groups in these conditions.

In summary, the oxygen vacancies created during the activation step are responsible for activating molecular oxygen that remains adsorbed at room temperature and oxidizes CO at room temperature. The formed CO2 interacts with the surface sites resulting in carbonates and hydrogen carbonates that remain on the surface blocking the active sites. At temperatures high enough for the decomposition of CO3/HCO3− oxygen vacancies reappear and the catalytic activity increases. These ideas explain the behavior observed when the reaction is carried out in isothermal conditions (see Fig. 4). In this figure, an initial conversion occurs for 0, 20, 100 and 300 °C. Considering the proposed model, the initial oxidation rate is explained by the presence of adsorbed peroxide species, but the active sites are poisoned by the reaction product, carbon dioxide, through the formation of CO3/HCO3− species whose decomposition is not favored at this temperature resulting in a continuous decrease of the reaction rate. On increasing the reaction temperature, this effect is less noticeable and poisoning effect is less pronounced. At temperatures above 100 °C thermal decomposition of bicarbonate species proceeds (see Figs. 7 and 8) and the deactivation phenomenon is not detected. The toxic effect of CO3/HCO3− has been previously reported [34] as well as the beneficial effect of water that favors the formation of hydrogen carbonate that decomposes at much lower temperatures than the carbonate species [35].

Despite the role of the support in the activation of molecular oxygen, the presence of gold is required to achieve high CO conversions as evidence by the low activity measured for the support (Fig. 3). It is well known that the CO adsorption is strongly favored if gold species are present on the surface [36]. Formation of oxygen vacancies in the support and the catalyst takes place in a similar way; therefore, peroxides are formed in presence of gaseous O2. At room temperature, CO may be weakly adsorbed in the structural channels of the rhabdophane structure probably interacting with acidic OH groups. Thus, this weakly adsorbed CO is oxidized by peroxide species resulting in the formation of carbonate/bicarbonate species that block the active sites hindering the

catalytic activity that falls down to zero once the adsorbed peroxide species are reacted. At higher temperatures the decomposition of the most stable carbonate species takes place and evolution of CO2 is observed as a result of the decomposition reaction.

4. Conclusions

Au/CePO4 catalysts are highly active in the reaction of CO oxidation at low temperature. The support itself presents, at room temperature, a CO conversion close to 70% as a result of the stoichiometric reaction between weakly adsorbed CO and peroxide species formed by molecular oxygen adsorption on oxygen vacancy sites. Using in situ DRIFTS-MS studies some aspects of the oxidation mechanism have been disclosed:

1.The dehydration of the support (rhabdophane structure) induces the generation of oxygen vacancies, able to react with gaseous oxygen to give peroxide species.

2.These species oxidize CO at room temperature producing CO2, which may form carbonates and hydrogen carbonates that act as reaction intermediates poisoning surface sites at low temperatures.

3.At higher temperatures the reaction intermediate decomposes, thereby, surface oxygen vacancies are regenerated and the catalytic activity increases.

References

[1] C.H. Tseng, T.C.K. Yang, H.E. Wu, H.C. Chiang

J. Hazard. Mater., 166 (2009), p. 686

[2] M. Haruta, T. Kobayashi, H. Sano, N. Yamada

Chem. Lett., 16 (1987), p. 405

[3] W.Y. Hernández, M.A. Centeno, F. Romero-Sarria, J.A. Odriozola

J. Phys. Chem. C, 113 (2009), p. 5629

[4] M.I. Domínguez, M. Sánchez, M.A. Centeno, M. Montes, J.A. Odriozola

Appl. Catal. A, 302 (2006), p. 96

[5] M.A. Centeno, C. Portales, I. Carrizosa, J.A. Odriozola

Catal. Lett., 102 (2005), p. 289

[6] J.C. Fierro-González, J. Guzmán, B.C. Gates

Topics Catal., 44 (2007), p. 103

[7] V.C. Schwartz, D.R. Mullins, W. Yang, B. chen, S. Dai, S.H. Overbury

J. Phys. Chem. B, 108 (2004), p. 15782

[8] M.M. Schubert, S. Hackenberg, A.C. van Veen, M. Muhler, V. Plzak, R.J. Behm

J. Catal., 197 (2001), p. 113

[9] U.R. Pillai, S. Deevi

Appl. Catal. A, 299 (2006), p. 266

[10] F. Arena, P. Famulari, G. Trunfio, G. Bonura, F. Frusteri, L. Spadaro

Appl. Catal. B, 66 (2006), p. 81

[11] H. Liu, A.I. Kozlov, A.P. Kozlova, T. Shido, K. Asakura, Y. Iwasawa

J. Catal., 185 (1999), p. 252

[12] M.I. Domínguez, F. Romero-Sarria, M.A. Centeno, J.A. Odriozola

Appl. Catal. B, 87 (2009), p. 2445

[13] Y-F. Han, N. Phonthammachai, K. Ramesh, Z. Zhong, T. White

Environ. Sci. Technol., 42 (2008), p. 908

[14] A. Wang, H. Yin, D. Liu, H. Wu, M. Ren, T. Jiang, X. Cheng, Y. Xu

Mater. Lett., 61 (2007), p. 2084

[15] W. Yan, S. Brown, Z. Pan, S.M. Mahurin, S.H. Overbury, S. Dai

Angew. Chem. Int. Ed., 45 (2006), p. 3614

[16] R.C.L. Mooney

Acta Cryst., 3 (1950), p. 337

[17] Z. Kónya, V.F. Puntes, I. Kiricsi, J. Zhu, J.W. Ager, M.K. Ko, H. Frei, P. Alivisatos, G.A. Somorjai

Chem. Mater., 15 (2003), p. 1242

[18] S. Lucas, E. Champion, D. Bernache-Assollant, G. Leroy

J. Solid. State Chem., 177 (2004), p. 1312

[19] H. Assaaoudi, A. Ennarici, A. Rulmoat

Vib. Spectrosc., 25 (2001), p. 81

[20] C. Corsaro, V. Crupi, D. Majolino, S.F. Parker, V. Venuti, U. Wanderlingh

J. Phys. Chem. A, 110 (2006), p. 1190

[21] M.I. Domínguez, P. Navarro, F. Romero-Sarria, D. Frías, S.A. Cruz, J.J. Delgado, M.A. Centeno, M. Montes, J.A. Odriozola

J. Nanosci. Nanotechnol., 8 (2008), p. 1

[22] M. Markovic, B.O. Fowler, M.S. Tung

J. Res. Natl. Inst. Stand. Technol., 109 (2004), p. 553

[23] H.H. Adler

Am. Mineral., 49 (1964), p. 1002

[24] E.C. De Cario, J.C. Edwards, T.R. Scalzo, D.A. Storm, J.W. Bruno

J. Catal., 132 (1991), p. 498

[25] F. Romero-Sarria, L.M. Martínez T., M.A. Centeno, J.A. Odriozola

J. Phys. Chem. C, 111 (2007), p. 14469

[26] M. Li, Z. Wu, Z. Ma, V. Schwartz, D.R. Mullins, S. Dai, S.H. Overbury

J. Catal., 266 (2009), p. 98

[27] C. Binet, M. Daturi, J.C. Lavalley

Catal. Today, 50 (1999), p. 207

[28] J.C. Lavalley

J. Catal., 27 (1996), p. 377

[29] G.C. Bond, D.T. Thompson

Gold Bull., 33 (2000), p. 41

[30] G.C. Bond, D.T. Thompson

Gold Bull., 42 (2009), p. 247

[31] O.H. Laguna, F. Romero-Sarria, M.A. Centeno, J.A. Odriozola

J. Catal., 276 (2010), p. 360

[32] T. Itoh, T. Maeda, A. Kasuya

Faraday Discuss., 132 (2006), p. 95

[33] S. Rossignol, F. Gérard, D. Duprez

J. Mater. Chem., 9 (1999), p. 1615

[34] M. Daté, M. Okumura, S. Tsubota, M. Haruta

Angew. Chem. Int. Ed., 43 (2004), p. 2129

[35] F. Romero-Sarria, A. Penkova, L.M. Martinez T., M.A. Centeno, K. Hadjiivanov, J.A. Odriozola

Appl. Catal. B, 84 (2008), p. 119

[36] A. Sánchez, S. Abbet, U. Heiz, W.D. Schneider, H. Häkkinen, R.N. Barnett, U. Landman

J. Phys. Chem. A, 103 (1999), p. 9573

Figure captions

Figure 1. XRD diagrams of CeP calcined at 300 and 950 °C.

Figure 2. TEM micrographs of the support (A) and the catalyst (B).

Figure 3. Light-off curves corresponding to CeP and AuCeP

Figure 4. CO conversion as a function of the time at different temperatures

Figure 5. Profile of water during the activation of the support

Figure 6. Difference spectra during the activation of the catalyst.

Figure 7. Difference spectra during the reaction (AuCeP).

Figure 8. Difference spectra during the reaction (AuCeP, extended 1800–700 cm−1 region).

Table 1

Table 1. Chemical composition and textural properties of the studied solids.

Sample	Chemical composition (wt.%)				Textural properties		
	O	P	Au	Ce	S_{BET} ($m^2\ g^{-1}$)	Vp ($cm^3\ g^{-1}$)	Dp (Å)
CeP	32.78	10.22	0	56.94	107	0.33	107.6
AuCeP	34.96	10.98	1.17	52.76	95	0.30	112.6

Figure 1

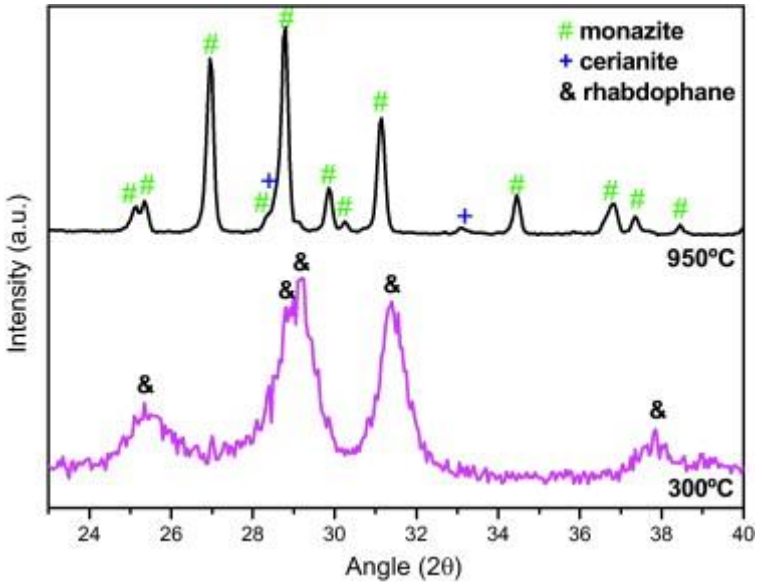
monazite
+ cerianite
& rhabdophane
950°C
300°C
Intensity (a.u.)
Angle (2θ)
24
26
28
30
32
34
36
38
40

Figure 2

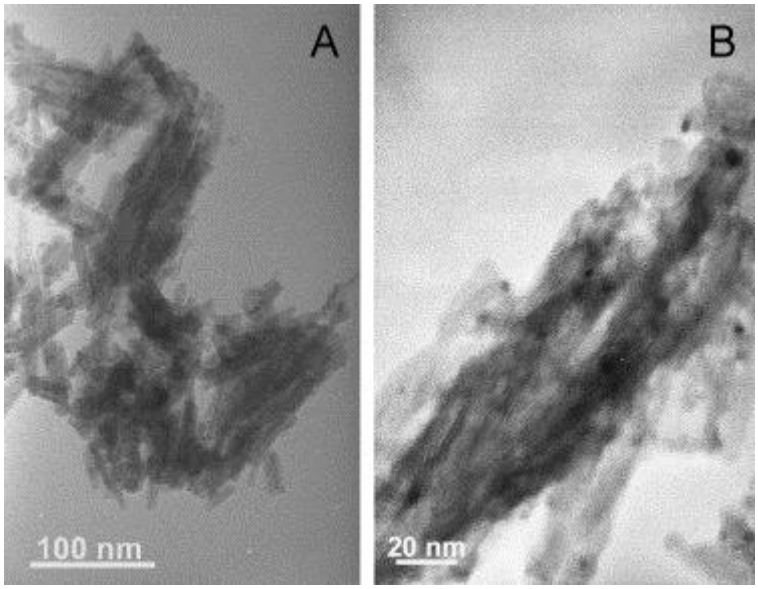

Figure 3

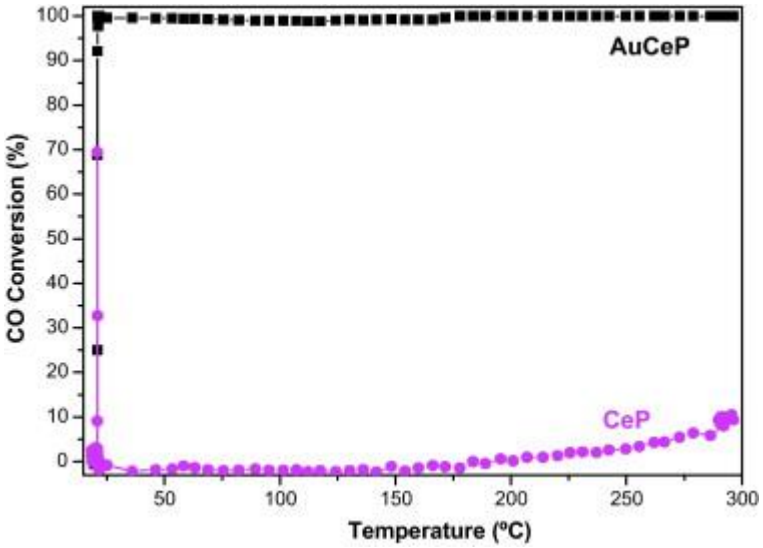
AuCeP
CeP
CO Conversion (%)
Temperature (ºC)
0
10
20
30
40
50
60
70
80
90
100
50
100
150
200
250
300

Figure 4

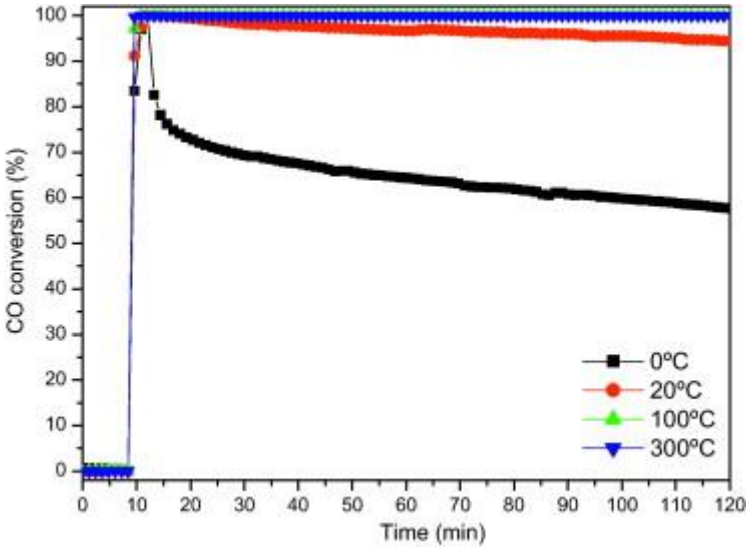

Figure 5

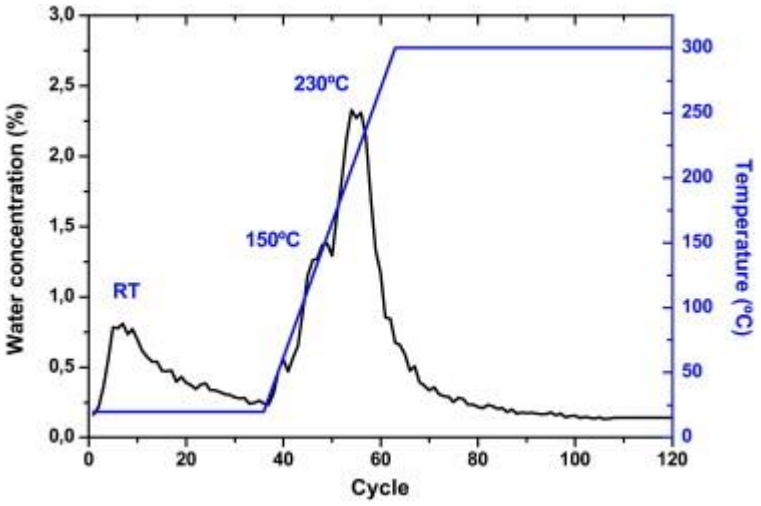
Water concentration (%)
Temperature (°C)
Cycle
RT
150°C
230°C
3,0
2,5
2,0
1,5
1,0
0,5
0,0
300
250
200
150
100
50
0
0
20
40
60
80
100
120

Figure 6

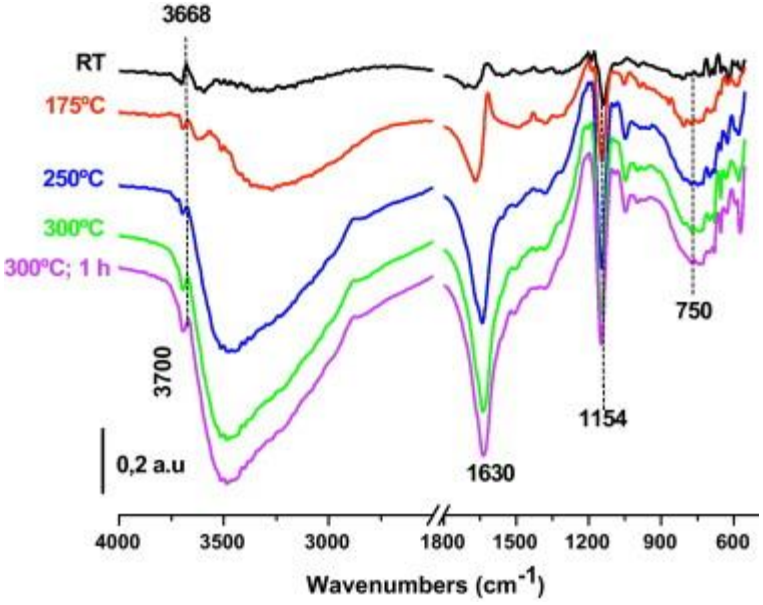
3668
RT
175ºC
250ºC
300ºC
300ºC; 1 h
3700
0,2 a.u
1630
1154
750
4000
3500
3000
1800
1500
1200
900
600
Wavenumbers (cm-1)

Figure 7

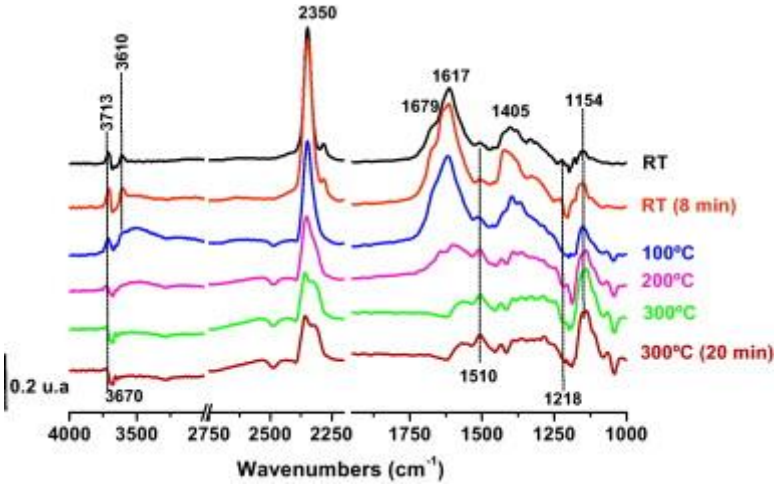
2350
3610
3713
1617
1679
1405
1154
RT
RT (8 min)
100°C
200°C
300°C
300°C (20 min)
0.2 u.a
3670
1510
1218
4000
3500
2750
2500
2250
1750
1500
1250
1000
Wavenumbers (cm-1)

Figure 8

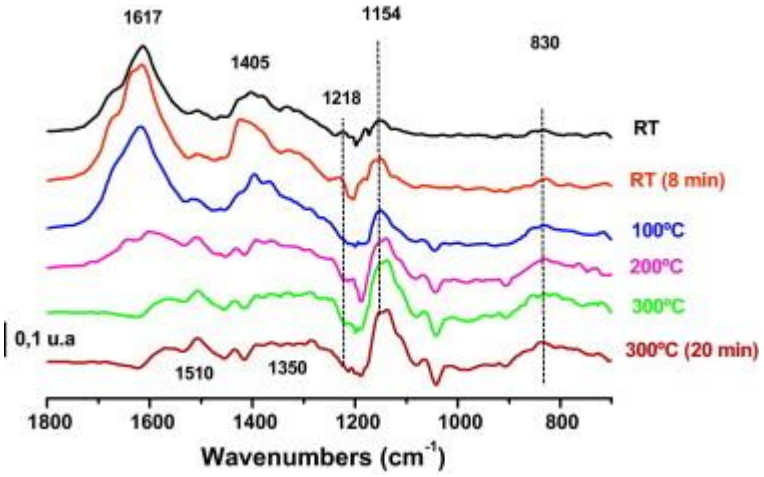
1617
1405
1218
1154
830
RT
RT (8 min)
100°C
200°C
300°C
300°C (20 min)
0,1 u.a
1510
1350
1800
1600
1400
1200
1000
800
Wavenumbers (cm-1)